SUNGLITTER IMAGERY OF THE OCEAN SURFACE PHENOMENA

Alexander Myasoedov [1, 2], Vladimir Kudryavtsev [1, 2], Bertrand Chapron [3], Johnny Johannessen [4]

[1]NIERSC, 7, 14th Line, office 49; Vasilievsky Island, 199034 St. Petersburg, RUSSIA,
Email: alexander.myasoedov@gmail.com
[2]RSHU, Malookhtinsky prospect 98, St. Petersburg, RUSSIA,
Email: kudr@rshu.ru
[3] IFREMER, Ifremer Technopôle Brest-Iroise BP 70, 29280 Plouzané, FRANCE,
Email: Bertrand.Chapron@ifremer.fr
[4]NERSC, Thormøhlensgt. 47 N-5006, Bergen, NORWAY,
Email: johnny.johannessen@nersc.no

ABSTRACT

An algorithm for retrieval of spatial variations of the mean square slope (MSS) of the sea surface from sunglint imagery is proposed. The retrieval algorithm is free on a prior suggestion on PDF model. The transfer function, relating the brightness contrast to the MSS contrasts, is found from observed sunglint brightness, where "real" PDF of the sea slopes has built-in. Developed approach was applied for analysis of the sunglint signature of the mesoscale ocean dynamics and internal waves. We found that the ocean currents (eddies, meanders, frontal lines) and internal waves are well visible on the sea surface as the MSS anomalies. Results of this study is further adopted by Kudryavtsev et al. (2010) for development of advanced approach for synergetic use of SAR and optical imagery in studies of meso-scale ocean dynamics.

1. INTRODUCTION

One of the main oceanographic applications of the data from the satellite optical scanners (e.g. from MODIS, MERIS) is the ocean color studies (e.g. Doerffer and Schiller, 2007). In these studies the sunlight reflected from the sea surface, is considered as a noise that must be removed. In the sun glitter area the radiation reflected constitute the major part of the upward radiation and its removal provides significant difficulties in development of the ocean color algorithms.

On the other hand, the sun glitter possesses the valuable information on statistical properties of the sea surface - its mean square slope (MSS), skewness and kurtosis as demonstrated by Cox and Munk (1954a, 1954b and 1956), and recently reported by Bréon and Henriot (2006), using a large collection of optical satellite observations. Since sunglint brightness depends on the MSS, any sea surface phenomenon (slicks, internal waves or currents boundaries) leading to the MSS variations becomes visible in the form of the brightness contrast. Cox and Munk (1954a,b) using the sunglint imagery investigated impact of artificial surface films on MSS. Jackson (2007) reported use of MODIS sunglint imagery for the internal wave detection and their survey over the world ocean. Bolshakov et al (1990) proposed the method for retrieval of 2D spectrum of the dominant surface waves elevations from the photograph of the sun glitter. Thus existing studies have demonstrated potential capability of sunglint imagery for detection of a number of dynamical oceanic phenomena, like slicks, internal and surface waves, current features.

The space optical scanners (e.g. MODIS, MERIS) produce almost daily worldwide coverage which results in a large volume of imagery that has sunglint. In this context the optical sensors can be considered as the instruments complementary to the SAR that may potentially be used for the oceanic surface phenomena survey on a near-global scale. In spite of numerous efforts, the physics of SAR imaging of the ocean phenomena is not properly investigated and the mechanisms leading to manifestation of the ocean phenomena on the sea surface are still poorly understood. In order to better understand physics of surface manifestation, a new "SAR-independent" data source on the surface signatures is desirable. Sunglint imagery opens such opportunity. In this case, there is a possibility to analyze surface signatures in terms of fundamental parameter of the sea surface roughness, - its MSS.

The goals of the present study are to develop a method for quantification of the surface signatures in terms of the MSS anomalies, and to demonstrate ability of the proposed method for quantitative estimates of the MSS signatures of the meso-scale currents and internal waves.

2. RETRIEVAL OF THE MSS VARIATIONS

2.1. The data

This study is focused to the MODIS imagery. The MODIS data are acquired at 36 channels in the visible and infrared range, with a spatial resolution between 250 m and 1 km and with a geolocation accuracy of at least 60 m (Salomonson et al., 1989). The MODIS images collected during the daylight period contain

distinctive silvery-gray ellipses of reflected sunlight over the oceans where view angle is within approximately 30 degree off the Sun's specular reflection point. Very these sunglint regions, where standard ocean color products cannot be retrieved (Esaias et al., 1998), could be the most favorable for detection of ocean phenomena through their surface manifestation.

We suggest that the red channel is the most preferable for sunglint imagery, because the light in the red channel is absorbed in a "thin" surface layer (Jerlov, 1976) and thus not too sensitive to the "color" of the water column, and does not dependent on the sea surface temperature. We use the Level 1B 250m resolution MODIS data in 645nm and 850nm channels accompanied with geolocation, "view and sun geometry" data.

Due to the scanning mirror construction, the MODIS image represents a composition of the stripes. Each strip is formed by 40 detectors with the along track field of view about 0.8 deg and cross track field of view about 110 deg. This instrument view geometry forms a strip with the ground dimensions of 2330 km length and about 10 km width at nadir. Thus each of the strips provides 2D field of the surface brightness. Inside the sunglint these peculiarities of the MODIS imagery may produce step-like changes of the sea surface brightness. The algorithm of the MODIS data processing in the sunglint area is designed as a strip-processing one, i.e. the whole images is divided on the strips which are then processing strip by strip. The brightness field B of each of the strips is decomposed on two parts, - large $\overline{B}$ and small $\tilde{B}$ scale parts, i.e. $B = \overline{B} + \tilde{B}$. Field $\overline{B}$ corresponds to variability of the brightness on scale of the sunglint width, and field $\tilde{B}$ contains brightness variations $\tilde{B}$ on the inner (much smaller) scales, which can be treated as the brightness signatures of sub- and meso-scale oceanic phenomena as well as wind filed variability.

2.2. The mean square slope variations

The sea surface radiance B generated by specular reflection of the sun light is (Cox and Munk, 1954a,b)

$$B \equiv I \cdot \cos\theta_v = \frac{\rho E_0}{4\cos^4\beta} P(Z_x, Z_y) \qquad (2.1)$$

where I is reflected radiance, E_0 is the solar irradiance, ρ is Fresnel reflection coefficient, θ_v is view zenith angle, P is the 2D probability density function (PDF) of the sea surface slopes z_x and z_y, and capital Z_x and Z_y denote the sea surface slopes satisfying to the conditions of the specular reflections of the sun light to the sensor

$$Z_x = -\frac{\sin\theta_s \cos\varphi_s + \sin\theta_v \cos\varphi_v}{\cos\theta_s + \cos\theta_v}$$
$$Z_y = -\frac{\sin\theta_s \sin\varphi_s + \sin\theta_v \sin\varphi_v}{\cos\theta_s + \cos\theta_v} \qquad (2.2)$$

here θ_s is the sun zenith angle, φ_v and φ_s are view and sun azimuth, and

$$\tan\beta = \sqrt{Z_x^2 + Z_y^2} \qquad (2.3)$$

is the surface slope related to Z_x and Z_y.

Eq. (2.1) to be treated as the fundamental one and any suggestions could only be made for the PDF. Cox and Munk (1954a,b) and later e.g. Chapron et al., 2000; Ebuchi and Kizu, 2002; Bréon and Henriot, 2006, suggested to model the PDF as a Gram-Charlie series. Fitting this PDF model to the observed sunglint, Cox and Munk (1954a,b) derived fundamental statistical properties of the sea surface slopes, - mean square slopes, skewness and peakedness, and established their dependence on wind speed. On the other hand, relation (2.1) provides an additional opportunities to investigate the sea surface phenomena (e.g. surface slicks, current features) leading to variations of the MSS and thus sunglint radiance on the inner scales, i.e. on the scales much smaller than the sunglint "width".

In order to avoid a specification of a model for the PDF, let us suggest that P in (2.1) is represented as

$$P(Z_x, Z_y) = s^{-2} p(\xi, \eta) \qquad (2.4)$$

where $\xi = Z_x / s$ and $\eta = Z_y / s$, s^2 is the mean square slope, and p is a "dimensionless" PDF. Certainly, being a function of ξ and η, function p possesses the up/down wind asymmetry of the surface slopes, as well as their non-linear peculiarities, - skeweness and peakedness. Notice that if PDF is specified e.g. by the Gaussian PDF or Gram-Charlie series, then "dimensionless" p in (2.4) can be found easily. However, as we show below, targeting on development of an algorithm for retrieval of the MSS contrast from the sunglint brightness, we do not need an *a priori* specified PDF model, but we may use its "real" form which is explicitly built-in the shape of the sunglint.

We suggest that MSS, s^2, (as well as other characteristics of the surface slopes) can be represented as a sum of a mean value $\overline{s^2}$ and its variations $\widetilde{s^2}$

$$s^2 = \overline{s^2} + \widetilde{s^2} \qquad (2.5)$$

Variations $\tilde{s}^2$ take place on the inner spatial scale l which is much smaller than suglint scale L: $l << L$. Hereinafter the bar over mean quantities is omitted. Eqs. (2.1) and (2.4) straightforwardly give us the following linearized relation between small variations of the sunglint brightness $\tilde{B}$ and the MSS, $\tilde{s}^2$:

$$\frac{\tilde{B}}{B} = -T\frac{\tilde{s}^2}{s^2}$$
$$T = 1 + \frac{1}{2}\left(\frac{\xi}{p}\frac{\partial p}{\partial \xi} + \frac{\eta}{p}\frac{\partial p}{\partial \eta}\right) \qquad (2.6)$$

where T is the transfer function. To derive (2.6) we have assumed that $\tilde{s}^2$ dominates variations of other statistical parameters of the sea surface slopes, in particular, its skewness and peakedness. By other words, we assume that magnitude of the relative MSS variations $\tilde{s}^2 / s^2$ is significantly larger than relative variations of the normalized momentum of the sea surface slopes $c_{mn} = \overline{z_x^m z_y^n} / s^{m+n}$: $\tilde{s}^2 / s^2 \gg \tilde{c}_{mn} / c_{mn}$. This assumption is supported by Cox and Munk (1954a,b) data for MSS of clean and slick covered surface. According to their measurements, the ratio of the MSS for clean and slick area at wind speed 4-15m/s is about $(s^2)_{clean} / (s^2)_{slick} \approx 2$, while for the normalized momentum c_{20} (up-wind component of the MSS) and c_{02} (cross-wind component of the MSS) the similar ratios $(c_{20})_{clean} / (c_{20})_{slick}$ and $(c_{02})_{clean} / (c_{02})_{slick}$ are varied within 1 ± 0.1. These estimates show that though MSS is strongly suppressed in the slick areas, the coefficients of the slope anisotropy vary insignificantly.

In order to determine the transfer function T one needs to find the gradients of the "dimensionless" PDF p in (2.6). There are two options: first one is to specify the model PDF, to fit it to observed sunglint and then to calculate T; the second option is to use observed shape of the sun glitter in order to determine the transfer function empirically. The latter option seems more attractive since it does not require a prior suggestion on shape of the PFD model with posterior determination of the surface slopes moments defining the PDF. For example, we one suggests that the PDF model may be approximated by the Gaussian PDF for isotropic surface slopes, then $p \propto \exp(\xi^2 + \eta^2)$ and eq. (2.6) is reduced to

$$T = 1 - \left(Z_x^2 + Z_y^2\right) / s^2 \qquad (2.7)$$

where s^2 to be defined through the fitting of the brightness model (2.1) with (2.4) to observed sunglint. However, the quality of the MSS contrasts retrieval depends thoroughly on validity of the model PDF.

In the present study we determine the transfer function (2.6) through the large scale brightness gradients which can directly be available from the sunglint imagery. With use of (2.1) the gradients of the "dimensionless" PDF p in (2.6) can be found from the large scale sunglint brightness as

$$\frac{\xi}{p}\frac{\partial p}{\partial \xi} = \frac{\xi}{B}\frac{\partial B}{\partial \xi} - \frac{4Z_x^2}{1 + Z_x^2 + Z_y^2}$$
$$\frac{\eta}{p}\frac{\partial p}{\partial \eta} = \frac{\eta}{B}\frac{\partial B}{\partial \eta} - \frac{4Z_y^2}{1 + Z_x^2 + Z_y^2} \qquad (2.8)$$

Due to the scanning mirror construction, the MODIS image represents a composition of the stripes (see Fig. 1). Each strip is formed by 40 detectors with the along track field of view about 0.8 deg and cross track field of view about 110 deg. This instrument view geometry forms a strip with the ground dimensions of 2330 km length and about 10 km width at nadir. Thus each of the MODIS strips provides 2D field of the surface brightness.

As mentioned, the MODIS image consists of the strips providing the data on 2D brightness gradients. In this case brightness gradient in (ξ, η)- space in (2.6) can be expressed through along-strip $(\nabla_l B)$ and cross-strips $(\nabla_n B)$ brightness gradients available from the MODIS imagery as:

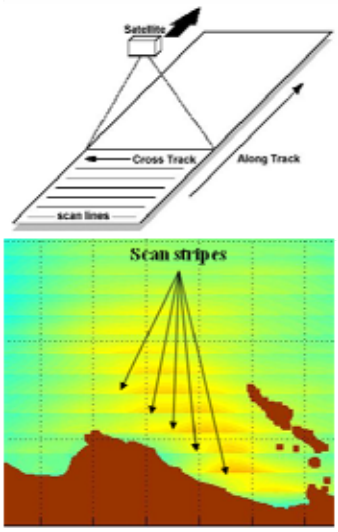

Figure 1. Upper plot: Schematic satellite viewing geometry. Lower plot: MODIS/Aqua cropped image of the Agulhas area dated 17th November 2007 at 12h05m providing along- and cross-track gradients of the surface reflected brightness over the glitter area. Brown colour masks the land.

$$\frac{\xi}{B}\frac{\partial B}{\partial \xi} = Z_x \frac{\nabla_l \ln B \cdot \nabla_n Z_y - \nabla_n \ln B \cdot \nabla_l Z_y}{\Delta}$$
$$\frac{\eta}{B}\frac{\partial B}{\partial \eta} = Z_y \frac{\nabla_n \ln B \cdot \nabla_l Z_x - \nabla_l \ln B \cdot \nabla_n Z_x}{\Delta} \qquad (2.9)$$

where discriminant Δ is

$$\Delta = \nabla_l Z_x \cdot \nabla_n Z_y - \nabla_n Z_x \cdot \nabla_l Z_y \qquad (2.10)$$

Thus, eqs. (2.6) with (2.8) and (2.9) represent an algorithm for retrieval of the sea surface MSS contrasts caused by arbitrary surface phenomenon through measured sunglint brightness and its variations on the inner scale. Proposed algorithm is free of any suggestions on *a prior* specification of the PDF model and can be applied for analysis of any type of images which provide 2D field of the sun glitter brightness.

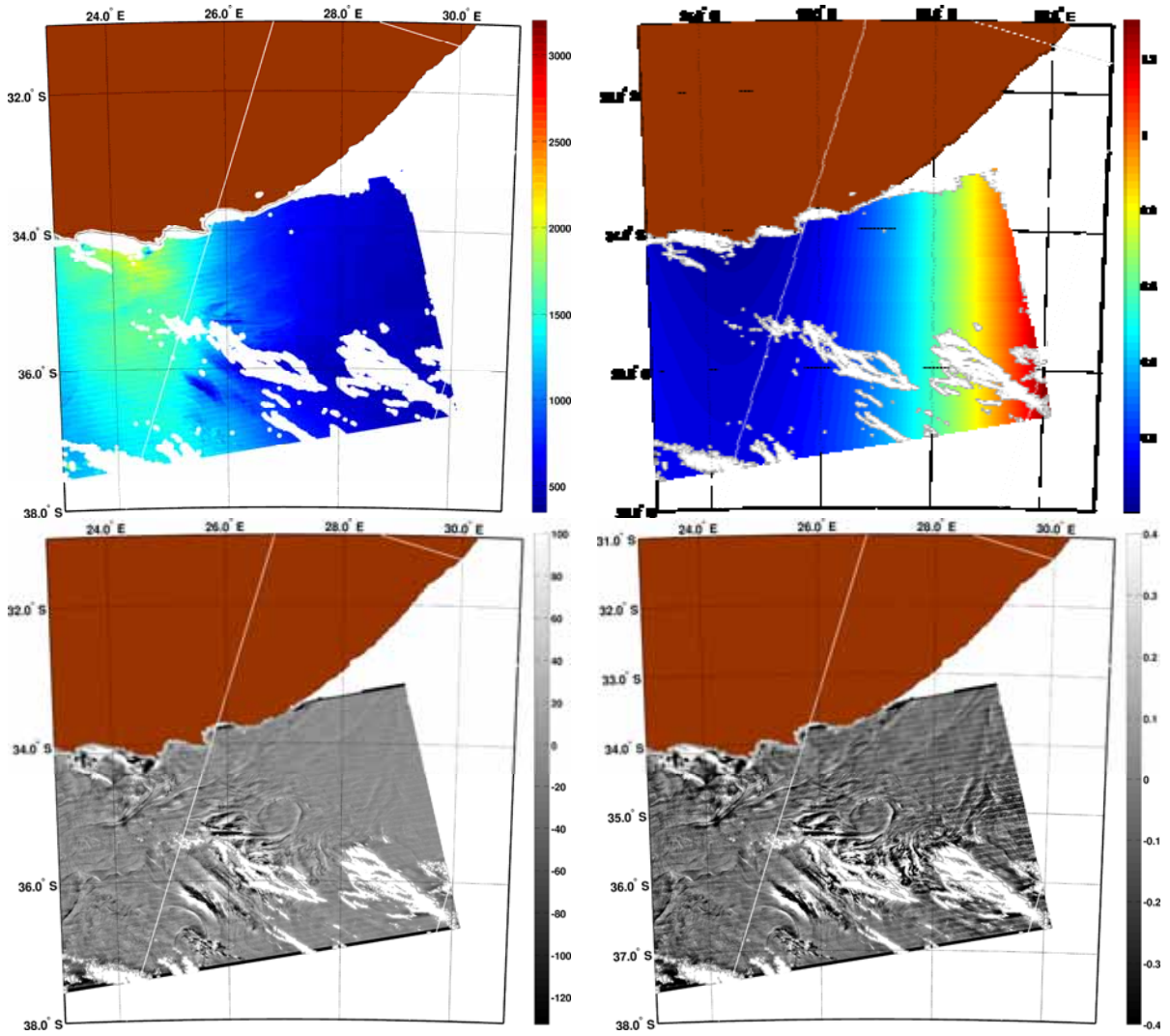

Figure 2. The Aqua/MODIS image of 250m resolution red channel of the Agulhas current area on the 18th November 2007, 12h05m. Original image is shown in the upper-left plot, and the brightness variations are in the lower-left plot. Upper-right plot shows the transfer function defined by eq. (2.6), and the lower-right plot is the field of the MSS variations calculated using eq. (2.6). Notice a strip-like structure of the sunglint area which is typical for the MODIS imagery. White areas are the clouds mask, and brown – the land. White square overlaying the images is the Envisat ASAR WS image overlaying the same area in the morning 7h24m the same day.

3. CASES STUDY

3.1. The Agulhas case study

The area of the intensive Agulhas current characterized by variety of the mesoscale dynamical patterns (currents, eddies, mushroom structures, fronts, internal waves etc), and representing favorable conditions for the sunglint imagery was chosen as the best test area for the present study.

An original Aqua/MODIS image in red channel (645nm) on 18 Nov 2007 12h05m is shown in Fig. 2 (upper-left plot). Clouds and land masks, and the sunglint on the ocean surface can easily be recognize. The remarkable feature is a strip-like structure of the sunglint area typical for the MODIS imagery. Note also a brightness feature on the "right slope" of the sunglint, close to the cloud mask which may presumably be treated as the ocean eddy signature.

The image was processed using the algorithm and appropriate software described in section 2.2. Original image was decomposed on the smoothed brightness $\bar{B}$ (not shown here) and its variations $\tilde{B}$; the latter is shown in Fig. 2, lower-left plot, and it exhibits apparent sunglint signatures of the ocean current. The transfer function defined by (2.6) and calculated for the smooth brightness filed is shown in Fig. 2, upper-right plot. The transfer function is positive therefore sign of the brightness contrasts corresponds to the sign of the MSS one. Lower-right plot in Fig. 2 shows field of the MSS contrasts retrieved from the brightness fields shown in Fig. 2, lower-left plot, with use of eqs. (2.6), (2.8) and with the transfer function shown in the upper-right plot.

Amplitudes of the MSS contrasts are "statistically" uniform over the observed area, except for local areas adjacent to the clouds where the sunglint brightness is presumably "contaminated" by the cloud shadiness, and thus suggested algorithms is not valid in these areas.

Surface signatures of the ocean currents are surprisingly well visible in the sea surface MSS: coupled eddies, meanders, and frontal linear features. A typical magnitude of the MSS contrasts is about 20-30%, and their shape has a form of sharp linear features, with width of 1 km order.

The MSS is formed by full range of wind surface waves, - in the wavelength range from 1mm to wavelength of the spectral peak (order of tens m) with dominant contribution from shortest waves. Therefore we may assume that MSS signatures are formed by short wind waves, with wavelength shorter than 1m.

3.2. Internal Waves

The western equatorial Atlantic region facing the mouth of the Amazon River is the area with very well-known regular occurrence of very intensive solitary and trains of internal waves (IWs) generated by semidiurnal tide (Ivanov et al., 1993). An extensive field measurements of IWs and their manifestations on the sea surface in this area were performed by Dulov et al. (1986). They found that during the peak generation, "amplitude" of the solitary IWs was about 100m, and that passage of the IW (travelling to the N-E direction, opposite to the wind) caused strong impact on the wind waves breaking. Waves breaking were strongly intensified (in few times relative to the background value) when the thermocline was deepening, and strongly suppressed (almost disappeared) when the thermocline was rising, i.e. wave breaking enhancement/suppression has strong correlation with convergence/divergence of the currents induced by the IW on the surface.

The MODIS/Aqua image of this area in red channel (645nm) on April 26, 2009, 16:20 is shown in Fig. 3, upper-left plot. Clouds mask, the sun glitter with linear brightness features inside (which may be treated as the surface signatures of the IWs) can easy be recognized.

The image was processed with use of the algorithm described in section 2.2. Fields of the smoothed brightness and its variations are shown in Fig. 3(upper-mid and upper right plots correspondingly). The smoothed image possesses the main features of the sunglint, while the brightness variations apparently contain sunglint signatures of the IWs.

The transfer function (2.6) calculated from smooth brightness (Fig. 3, upper-mid plot) is shown in Fig. 3, lower-mid plot. Unlike the Agulhas case, the transfer function is negative over the observed area. Thus sign of the brightness contrasts to be opposite to the sign of the MSS anomalies.

MSS anomalies retrieved from the smoothed brightness fields of eqs. (2.6) with the use of transfer function (calculated from (2.8) and (2.9)) shown in lower-mid plot of Fig. 3 is presented in Fig. 4. This figure apparently exhibits variety of the IW patterns. The main feature is a spatial recurrence of the IW patterns; each of the patterns begins from the leading solitary IW and following trains of IW with wavelengths 1km and 10km. The distance between leading solitons is about 150 km. Since IWs in this area are generated by semidiurnal tide, then the phase speed of IWs is about 3.5. m/s.

Fig. 5 (upper plot) shows profiles of the MSS variations along cross-sections A-B shown in Fig. 4. This figure illustrates additional features of the sea surface signature of IWs: first manifestation of the IW solitons in MSS has a "bi-polar" shape consisting of negative and positive MSS anomalies.

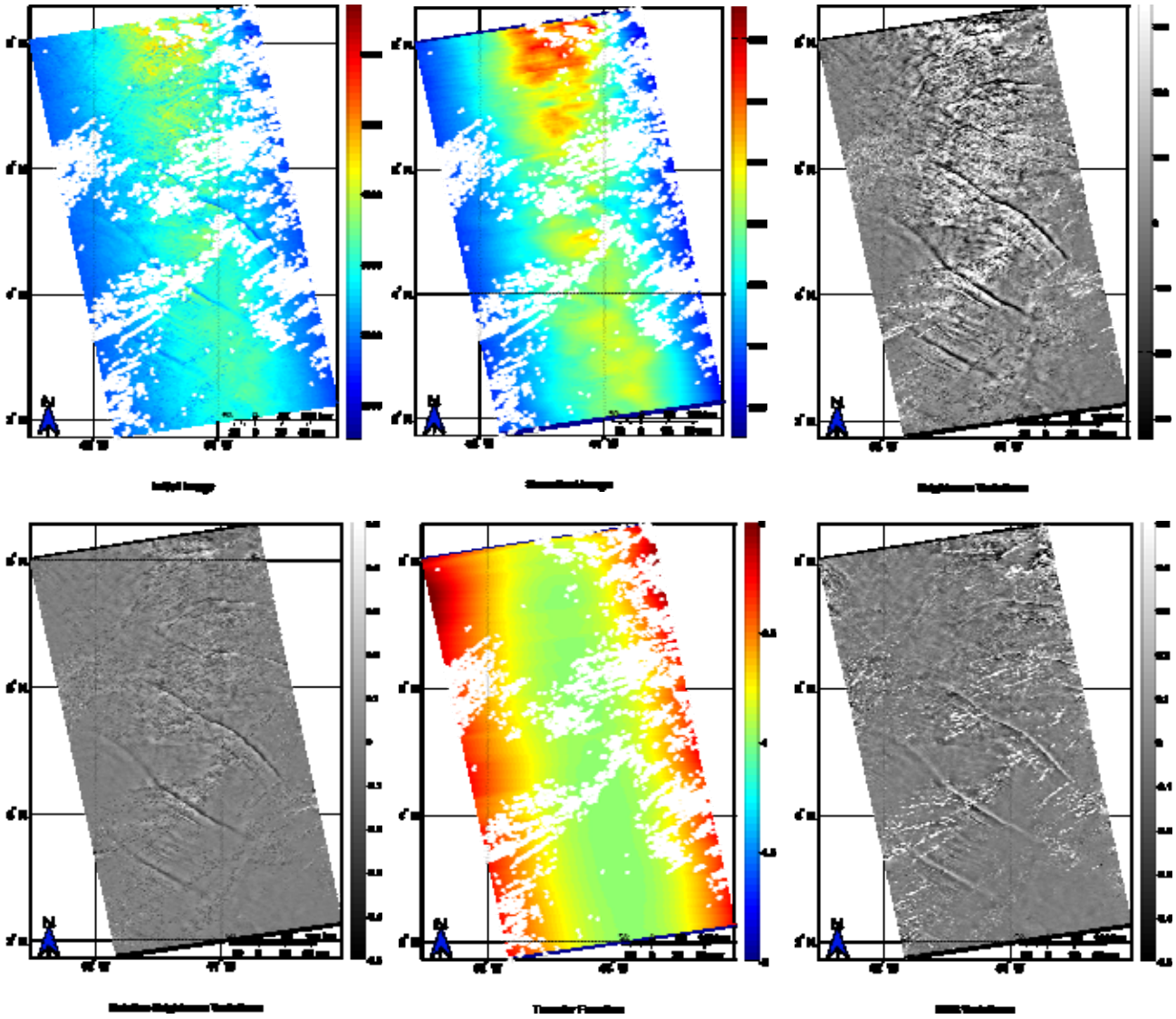

Figure 3. The Aqua/MODIS image red channel (645nm) of 250m resolution, Amazon Area on April 26, 2009, 16:20. Upper-left: fragment of the original MODIS image; upper-middle: smoothed image; upper-right: brightness variations; lower-left: relative brightness variations; lower-middle: the transfer function (2.6). lower-right: MSS contrasts field. White areas are the clouds mask.

Recalling the shape of the IW soliton, we may conclude that increase of the MSS takes place in the zone of IW-induced surface current convergence (above forward slope of the soliton) and decrease – in the zone of the current divergence, above the back slope of the soliton. Notice that location of the MSS anomalies is similar to manifestation of solitary IW in wave breaking, as observed by Dulov et al. (1986) in this area.

In order to check whether the observed IW-induced modulations of the sea surface MSS corresponds to the "real" one, we have performed the model simulation of the data shown in Fig. 5 using the radar imaging model (RIM) developed by Kudryavtsev et al (2005). RIM model had been extensively validated against available data on radar signature of IW, and has demonstrated its validity. As a first guess we assumed that observed increase/decrease in the MSS takes place in the convergence/divergence of the currents induced by IW on the sea surface, i.e. $K_s \equiv \widetilde{s^2} / s_0^2 \propto \partial u / \partial x$ where K_s is the contrast of the MSS.

The proportionality "constant" in this relation is a function (with dimension of time) depending on wind speed and its direction, IW characteristics (IW length, phase velocity), wind waves age and probably other parameters. Nevertheless, for the given condition it may be assigned as a tuning constant c_u, which have to be determined after comparison of observed MSS with model simulations.

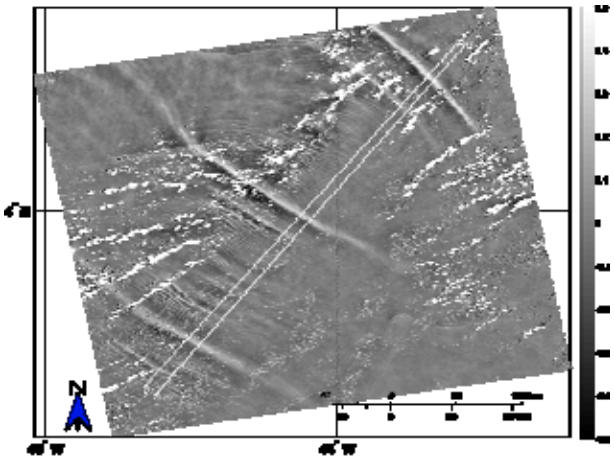

Figure 4. Field of the MSS contrasts depicting the surface signatures of the IW field. Lines A-B indicate location of the cross-sections shown in Fig. 5.

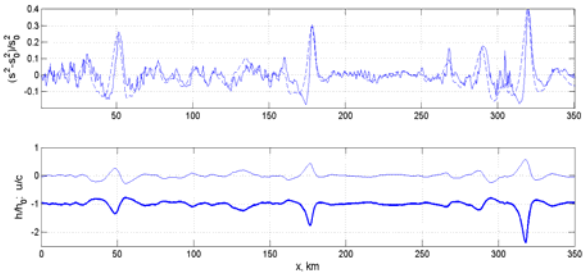

Figure 5. Upper plot: solid line,- profile of the MSS contrasts along cross-sections A-B shown in Fig. 4; dash line,- RIM simulation of the MSS contrasts for current velocity induced by IW on the surface shown by thin solid line in the lower plot. Displacement of the thermocline by IW is shown in the lower plot by thick solid lines. Current velocity is scaled by IWs phase velocity (3.5m/s), and thermocline depth is scaled by its undisturbed value.

Then the surface velocity can be assessed as

$$u(x) = c_u \int_0^x \left(K_s - \langle K_s \rangle \right) dx \qquad (3.1)$$

where $\langle K_s \rangle$ is "low frequency" oscillations in the MSS which are not visible in the data of Fig. 5, but may results in artificial contribution to $u(x)$ due to cumulative integration on (3.1). These oscillations can e.g. be caused by wind speed variability, and in our simulations are removed by fitting the polynomial of the 3d power to the MSS data.

Surface velocity (3.1) was specified as the input parameter for RIM simulations of surface signatures of IW travelling opposite to the wind with phase velocity $c = 3.5$. Wind speed was defined as 7 m/s. In these calculations the tuning constant c_u in eq. (3.1) was chosen to fit peaks of the model MSS variations associated with effect of the solitary IW to observed one. The model MSS are shown in Fig. 5, upper plot, by dash line. Note that in order to get right spatial location of the MSS peaks induced by solitary IWs, the model curve was shifted on 1 km to the right (towards IW direction). In the whole the model features of the IWs manifestation in the MSS are very similar to the observed modulations. This may justify the fact that real MSS modulations are governed by divergence of the surface current.

The reconstructed surface velocity profile as well as oscillations of the thermocline depth $h(x)$ are shown in Fig. 5, lower plot. The latter was found from the relation between surface velocity and the thermocline depth (within the frame of 2-layer density model with the shallow upper and the deep lower layers): $u / c = (h - h_0) / h$, where h_0 is the undisturbed depth, and c is IW phase velocity equal in our case to $c = 3.5$ m/s. Magnitudes of surface velocity oscillations and the thermocline layer displacement are consistent with field observations in this area. For example, Dulov et al. (1986) reported observations of wave breaking modulations by solitary IWs with amplitudes about 100m. If we assume that h_0 in our simulations is $h_0 = 100$ m, then amplitudes $h - h_0$ of two leading solitons in Fig. 5 are 120 m and 80 m, i.e. are in a quantitative agreement with observations. Thus we conclude that surface signatures derived from the sunglint imagery of IWs can be treated as reliable.

4. CONCLUSION

An algorithm for retrieval of the spatial variations of the MSS from the sunglint imagery has been proposed. The retrieval algorithm is free on a prior suggestion on spatial distribution of reflected sun radiance, e.g. - suggestion that it follows classical Cox and Munk model based on the PDF of the sea slopes described by the Gram-Charlie series. The transfer function, relating the brightness contrast to the MSS contrasts, is obtained on the basis of observed sunglint brightness gradient, where "real" PDF of the sea slopes has built-in.

Developed approach was applied for analysis of the sunglint signature of the mesoscale ocean dynamics and internal waves. Surface signatures of the ocean currents are surprisingly well visible in the sea surface MSS: coupled eddies, meanders, and frontal linear features. A typical magnitude of the MSS contrasts for the Agulhas study case is about 20-30%, and their shape has a form of sharp linear features, with width of 1 km order.

For more details on SAR and MODIS synergetic analysis of this case see (Kudryavtsev et al., 2010).

Developed approach proposes an additional opportunity for investigation of surface signature of ocean phenomena, including mesoscale ocean currents. We believe that synergetic analysis of the MSS (derived from optical sensors) and SAR surface signatures will lead to better understanding of the physics of sea

surface and mechanisms resulting in manifestation of the ocean phenomena on the sea surface.

Acknowledgements:
This work was supported by the Federal Targeted Program *"Research and scientific-pedagogical cadres of Innovative Russia"* for 2009-2013., in the framework of the activities № 1.3.2 "Targeted postgraduate students research", government contract № P1677.
Myasoedov A. and Kudryavtsev V. would like to acknowledge the support of the Research Council of Norway under the project 184778/S50 (MAREBASE).

5. REFERENCES

Bolshakov, A. N., V. M. Burdyugov, S. A. Grodskii, V. N Kudryavtsev, V. G. Proshchenko (1990), Spectra of energy-containing surface waves determined from sunglitter images. Comparison with in situ data. *Issledovaniye Zemli iz Kosmosa (English translations "Earth Observation from Space")*, 1, 19-27.

Bréon, F. M., and N. Henriot (2006). Spaceborne observations of ocean glint reflectance and modeling of wave slope distributions, *Journal of Geophysical Research*, 111, C06005, doi:10.1029/2005JC003343.

Chapron, B., V. Kerbaol, D. Vandemark, and T. Elfouhaily (2000). Importance of peakedness in sea surface slope measurements and applications, *J. Geophys. Res.,* 105, 17,195–17,202.

Cox, C., and W. Munk (1954a). Statistics of the sea surface derived from sun glitter. *J. Mar. Res.*, 13, 198–227.

Cox, C., and W. Munk (1954b). Measurement of the roughness of the sea surface from photographs of the Sun's glitter. *J. Opt. Soc. Amer.*, 44, 838–850.

Cox, C., and W. Munk (1956). Slopes of the sea surface deducted from photographs of sun glitter. *Bulletin of the Scripps Institution of Oceanography*, C. E. ZoBell, R. A. Arthur, and D. L. Fox, Eds., Vol. 6, No. 9, University of California Press, 401–488.

Doerffer, R. and Schiller, H. (2007). The MERIS Case 2 water algorithm. *Int. J. Remote Sens. 28*, 3-4 (Feb. 2007), 517-535, doi:10.1080/01431160600821127.

Dulov V., S. Klyushnikov, and V. Kudryavtsev, (1986). Effect of Internal waves on intensity of wind wave breaking. Field observation. *Morskoi Hydrofizicheskii Journal (English translation "Soviet Journal of Physical Oceanography")*, 6, 14-21

Ebuchi, N., and S. Kizu (2002). Probability distribution of surface slope derived using Sun glitter images from geostationary meteorological satellite and surface vector winds from scatterometers, *J. Oceanogr.*, 58, 477– 486.

Esaias, W. E., et al. (1998). An overview of MODIS capabilities for ocean science observations, IEEE Trans. *Geosci. Remote Sens.*, 36, 4.

Ivanov, V. A., E. N. Pelinovsky, and T. G. Talipova (1993). The long-time prediction of intense internal wave heights in the tropical region of the Atlantic, *J. Phys. Oceanogr.*, 23, 2136– 2142.

Jackson, C. (2007), Internal wave detection using the Moderate Resolution Imaging Spectroradiometer (MODIS), *Journal of Geophysical Research*, 112, C11012, doi:10.1029/2007JC004220.

Jerlov, N. G. (1976). *Marine Optics*. Elsevier Scientific Publishing Company, Elsevier Oceanography Series, 14.

Kudryavtsev V., D.Akimov, J.A.Johannessen, and B. Chapron (2005). On radar imaging of current features. Part 1: Model and comparison with observations, *Journal of Geophysical Research*, Vol. 110, C07017.

Kudryavtsev V. Myasoedov A., Chapron B., Johannessen J., Collard F. (2010). Synergy of SAR and optical imagery in studies of meso-scale ocean dynamics. Proc. 3rd SeaSAR workshop *'Advances in SAR Oceanography from ENVISAT, ERS and ESA third party missions'*, ESA SP679.

Salomonson, V. V., W. L. Barnes, P. W. Maymon, H. E. Montgomery, and H. Ostrow (1989). MODIS: Advanced facility instrument for studies of the Earth as a system, *IEEE Trans. Geosci. Remote Sens.*, 27, 145– 153.